Non-Bragg-gap solitons in one-dimensional Kerr-metamaterial Fibonacci heterostructures

E. Reyes-Gómez,[1] S. B. Cavalcanti,[2] and L. E. Oliveira[3]

[1]*Instituto de Física, Universidad de Antioquia UdeA, Calle 70 No. 52-21, Medellín, Colombia*
[2]*Instituto de Física, Universidade Federal de Alagoas, Maceió, Alagoas, 57072-970, Brazil*
[3]*Instituto de Física, Universidade Estadual de Campinas—Unicamp, Campinas, São Paulo, 13083-859, Brazil*

A detailed study of non-Bragg-gap solitons in one-dimensional Kerr-metamaterial quasiperiodic Fibonacci heterostructures is performed. The transmission coefficient is numerically obtained by combining the transfer-matrix formalism in the metamaterial layers with a numerical solution of the nonlinear differential equation in the Kerr slabs, and by considering the loss effects in the metamaterial slabs. A switching from states of no transparency in the linear regime to high-transparency states in the nonlinear regime is observed for both zero-order and plasmon-polariton gaps. The spatial localization of the non-Bragg-gap solitons is also examined, and the symmetry properties of the soliton waves are briefly discussed.

I. INTRODUCTION

The control and manipulation of light and its interaction with condensed matter have received a lot of attention in the last couple of decades. The study of photonic crystals (PCs) is essentially associated with the area of a new class of optical materials which display exciting and interesting properties with considerable practical applications, e.g., the challenge of constructing all-optical devices with the capability of replacing electronic transistors. The experimental realization of metamaterials [1] or left-handed materials (LHMs) [2] has opened up interesting possibilities in the study of one-dimensional (1D) plasmonic heterostructures. In this respect, both periodic and quasiperiodic structures, made up of bilayers AB composed of materials with positive (RHM) and negative (LHM) indices of refraction, have been the subject of both experimental and theoretical investigations [3]. Such periodic structures with metamaterial inclusions exhibit a non-Bragg band gap associated with the $\langle n \rangle = 0$ null average of the refractive index. Also, at the interface of the metamaterial and positive-refraction material, interactions between electromagnetic waves and the electronic plasma at the surface of the metamaterial may result in electromagnetic surface waves known as surface plasmon polaritons (SPPs) [4]. Moreover, recent investigations on one-dimensional RHM-LHM heterostructures have shown that, for oblique electromagnetic incidence, longitudinal bulklike plasmon polaritons (PPs) may be excited along the growth direction of the heterostructure with the non-Bragg PP gap showing up in the corresponding transmission spectra [5].

Theoretical studies on nonlinear layered systems have also revealed novel results [6,7]. Bragg-gap soliton solutions have been reported [8] for frequencies at the edge of the linear gap, in right-handed nonlinear materials in 1D superlattices which alternate linear and nonlinear media. Also, investigations [9] on alternate stacks of nonlinear-Kerr metamaterial have revealed the existence of a zero-order gap soliton: one finds a soliton-mediated transparency switching, from a state of no transparency in the linear regime to total transparency in the nonlinear regime. Recently, multistability, transmission switching, and n-soliton formation have been reported on Kerr-metamaterial superlattices at the band edge of the PP gap [10].

Properties intermediate between those of periodic and disordered systems are shown by quasiperiodic heterostructures. The band structure of 1D periodic and quasiperiodic stacks containing metamaterials strongly depends on the incidence angle [11–13]. Up to now, however, there appear to have been no investigations on the occurrence of transmission switching and soliton formation in the region of the non-Bragg $\langle n \rangle = 0$ and PP gaps of quasiperiodic photonic structures. Considering that the symmetry-breaking aspect of quasiperiodic structures has revealed a richer structure than its periodic counterpart, such as the unfolding of additional PP modes, a thorough investigation of the transmission switching and soliton formation phenomena in quasiperiodic metamaterial heterostructures with nonlinear inclusions is clearly in order.

Based on the above discussion, in the present study we investigate the nonlinear properties of non-Bragg $\langle n \rangle = 0$ and PP gaps in 1D Kerr-metamaterial quasiperiodic Fibonacci heterostructures. The work is organized as follows. Section II presents the theoretical framework and numerical results are given in Sec. III. Finally, the conclusions are in Sec. IV.

II. THEORETICAL FRAMEWORK

Here we are concerned with a heterostructured system composed by the building blocks A and B, which are arranged according to a Fibonacci sequence. The Fibonacci sequence S_m of order m may be constructed from the inflation law $S_m = S_{m-1}|S_{m-2}$ $(m \geqslant 2)$, with the initial conditions $S_0 = $ B and $S_1 = $ A. The symbol "|" represents a concatenation operation. For instance, one has $S_2 = $ AB, $S_3 = $ ABA, $S_4 = $ ABAAB, and so on. Alternatively, the Fibonacci sequence S_m may be obtained by replacing A $\to$ AB and B $\to$ A in S_{m-1}. A straightforward generalization allows one to see that the sequence S_m may also be obtained from the simultaneous substitutions A $\to$ S_{k+1} and B $\to$ S_k in the sequence S_{m-k}, where $0 \leqslant k \leqslant m$. For example, $S_{12} = S_{10}|S_9|S_{10}$, which results from the replacements A $\to$ S_{10} and B $\to$ S_9 in the sequence S_3. In the same way one may note that $S_{12} = S_9|S_8|S_9|S_9|S_8$, etc. A pictorial view of some Fibonacci sequences is displayed in Fig. 1. The total number F_m of elements A or B in the sequence S_m is determined by the general term of the Fibonacci succession $F_m = F_{m-1} + F_{m-2}$, with $F_0 = F_1 = 1$.
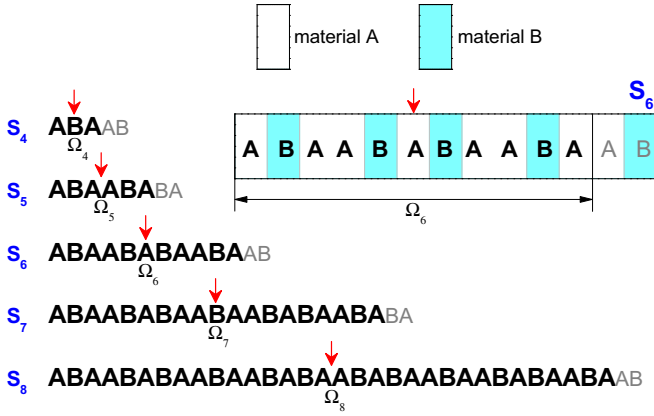
FIG. 1. (Color online) Pictorial view of some sequences S_m. The sequences Ω_m resulting from suppressing the two last elements of S_m (see the end of each sequence) are depicted as bold letters. Arrows indicate the approximate position of the inversion center of each Ω_m. A schematic representation of the building blocks A and B, as well as the Fibonacci heterostructure corresponding to the sequence S_6, is also displayed.

In addition, it is possible to see that the sequence Ω_m, resulting from suppressing the two last elements (AB or BA for even or odd values of m, respectively) of S_m, has an inversion center. This fact may be clearly observed from the schematic representation of the Fibonacci heterostructure corresponding to the sequence S_6 that we have drawn in Fig. 1.

In a Fibonacci heterostructure associated with the sequence S_m the symbols A and B represent slabs of different materials stacked along a certain preferential direction, say the z axis, and the building blocks A of width a and B of width b are made of a nonlinear Kerr material and a dispersive metamaterial, respectively. Here we note that, because of the quasiperiodic order of the Fibonacci sequence, the building block A in S_m may appear twice as AA, in which case the two corresponding Kerr slabs of width a are considered as a single Kerr slab of thickness $2a$. Layers A (or AA) are characterized by a constant magnetic permeability μ_A and an electric permittivity given by

$$\epsilon_A = \epsilon_A^0 + \alpha|E(z)|^2, \qquad (1)$$

where $E = E(z)$ is the electric-field amplitude of the electromagnetic field within the heterostructure. Slabs B represent the metamaterial, whose frequency-dependent electric permittivity and magnetic permeability are given by

$$\epsilon_B = f_\epsilon + \frac{F_\epsilon}{\beta_\epsilon - \nu^2 - i\nu\gamma} \qquad (2)$$

and

$$\mu_B = f_\mu + \frac{F_\mu}{\beta_\mu - \nu^2 - i\nu\gamma}, \qquad (3)$$

respectively. In the above expressions [9,10], we have set $f_\epsilon = 1.6$, $F_\epsilon = 40$ GHz^2, $\beta_\epsilon = 0.81$ GHz^2, $f_\mu = 1.0$, $F_\mu = 25$ GHz^2, and $\beta_\mu = 0.814$ GHz^2; ν is the linear frequency and γ is a phenomenological damping parameter which accounts for absorption and loss effects in the slabs B, both expressed in GHz.

Without loss of generality we have focused on the study of transverse-electric (TE) electromagnetic modes in the heterostructure. In this case one may show, by using the Maxwell equations [14], that the electric-field amplitude of the electromagnetic field satisfies the differential equation

$$-\frac{d}{dz}\left[\frac{1}{\mu(z)}\frac{d}{dz}E(z)\right] - \left[\frac{\omega^2}{c^2}\epsilon(z) - \frac{q^2}{\mu(z)}\right]E(z) = 0, \quad (4)$$

where $\epsilon(z)$ and $\mu(z)$ are the position-dependent electric permittivity and magnetic permeability of the heterostructure, respectively, $\omega = 2\pi\nu$, $q = \frac{\omega}{c}\sin\theta$ is the x component of the wave vector, and θ is the incidence angle relative to the vacuum. One may note that both E and $\frac{1}{\mu}\frac{d}{dz}E = \frac{1}{\mu}E'$ must be continuous functions at each interface between different materials. In the nonlinear Kerr material, Eq. (4) may be rewritten as

$$\frac{d^2}{d\xi^2}E(\xi) + \kappa_A^2 E(\xi) + \rho|E(\xi)|^2 E(\xi) = 0, \qquad (5)$$

where $\kappa_A^2 = \mu_A\epsilon_A^0 - \sin^2\theta$, $\rho = \mu_A\alpha$, and $\xi = \frac{\omega}{c}z$ is the reduced coordinate along the growth direction. In the metamaterial regions one has

$$\frac{d^2}{d\xi^2}E(\xi) + \kappa_B^2 E(\xi) = 0, \qquad (6)$$

with $\kappa_B^2 = \mu_B\epsilon_B - \sin^2\theta$.

The transmission coefficient of the heterostructure may be obtained by imposing radiative boundary conditions on the electromagnetic field in the external regions, i.e.,

$$E(\xi) = \begin{cases} E_i e^{i\kappa_0(\xi-\xi_0)} + E_r e^{-i\kappa_0(\xi-\xi_0)} & \text{if} \quad \xi < \xi_0, \\ E_t e^{i\kappa_0(\xi-\xi_{2N})} & \text{if} \quad \xi > \xi_{2N}, \end{cases} \quad (7)$$

where ξ_0 and ξ_{2N} correspond to the reduced coordinates of the beginning and end, respectively, of the S_m Fibonacci heterostructure, whereas E_i, E_r, and E_t are the amplitudes of the incident, reflected, and transmitted fields, respectively. In the above equation, $\kappa_0^2 = \mu_0\epsilon_0 - \sin^2\theta$, where μ_0 and ϵ_0 are the magnetic permeability and electric permittivity, respectively, of the medium surrounding the heterostructure. In the following, we choose $\mu_0 = \epsilon_0 = 1$ and, hence, $\kappa_0 = |\cos\theta|$.

We are interested in obtaining the reflection and transmission coefficients at a given value of the frequency ω. To this end, it is necessary to compute the amplitudes E_i and E_r for a given value of E_t [15,16]. In this way, one may solve both Eqs. (5) and (6) in the Kerr-material and metamaterial regions, respectively, and then apply the above-mentioned boundary conditions for the electric field at the interfaces. Let us exemplify this procedure for a Fibonacci heterostructure of even order m. In this case the Fibonacci sequence S_m always begins with the symbol A and ends up with the symbol B, and the reduced positions of the interfaces between different materials are labeled as $\xi_0, \xi_1, \ldots, \xi_{2N}$, where $N = F_{m-2}$. One may note that ξ_0 corresponds to the interface between vacuum and the first Kerr-material slab, whereas ξ_{2N} is the position of the interface between the last metamaterial slab and the vacuum region. Here we assume, for simplicity, $\xi_0 = 0$. The intervals (ξ_{2j-2}, ξ_{2j-1}) with $j = 1, 2, \ldots, N$ correspond to single (A) or double (AA) Kerr-material slabs, whereas

the intervals (ξ_{2j-1},ξ_{2j}) $(j = 1, 2, \ldots, N)$ correspond to the metamaterial regions. Of course, $\frac{\omega}{c} b = \xi_{2j} - \xi_{2j-1} = \bar{b}$.

In the metamaterial slabs, Eq. (6) may be solved analytically, and the corresponding solutions read

$$E_j(\xi) = C_j e^{i\kappa_B(\xi-\xi_{2j-1})} + D_j e^{-i\kappa_B(\xi-\xi_{2j-1})}, \qquad (8)$$

where C_j and D_j are the corresponding integration constants and $j = 1, 2, \ldots, N$. In the Kerr-material slabs, Eq. (5) may be solved numerically. Let us denote as f_j $(j = 1, 2, \ldots, N)$ the corresponding solutions for the electric field in the nonlinear regions. By taking into account the continuity of both E and $\frac{1}{\mu} E'$ at the interfaces, it is possible to show that

$$\begin{bmatrix} E_i \\ E_r \end{bmatrix} = -\frac{i}{2\kappa_0} \begin{bmatrix} i\kappa_0 & 1 \\ i\kappa_0 & -1 \end{bmatrix} \begin{bmatrix} f_1(\xi_0) \\ \frac{1}{\mu_A} f_1'(\xi_0) \end{bmatrix} \qquad (9)$$

in the first interface at ξ_0. In the interior of the heterostructure one has

$$\begin{bmatrix} f_j(\xi_{2j-1}) \\ \frac{1}{\mu_A} f_j'(\xi_{2j-1}) \end{bmatrix} = \begin{bmatrix} 1 & 1 \\ i\frac{\kappa_B}{\mu_B} & -i\frac{\kappa_B}{\mu_B} \end{bmatrix} \begin{bmatrix} C_j \\ D_j \end{bmatrix} \qquad (10)$$

with $j = 1, 2, \ldots, N$, and

$$\begin{bmatrix} f_j(\xi_{2j-2}) \\ \frac{1}{\mu_A} f_j'(\xi_{2j-2}) \end{bmatrix} = \begin{bmatrix} e^{i\kappa_B\bar{b}} & e^{-i\kappa_B\bar{b}} \\ i\frac{\kappa_B}{\mu_B}e^{i\kappa_B\bar{b}} & -i\frac{\kappa_B}{\mu_B}e^{-i\kappa_B\bar{b}} \end{bmatrix} \begin{bmatrix} C_{j-1} \\ D_{j-1} \end{bmatrix} \qquad (11)$$

with $j = 2, 3, \ldots, N$. By combining Eqs. (10) and (11) one may obtain

$$\begin{bmatrix} f_j(\xi_{2j-1}) \\ \frac{1}{\mu_A} f_j'(\xi_{2j-1}) \end{bmatrix} = \begin{bmatrix} \cos(\kappa_B\bar{b}) & -\frac{\mu_B}{\kappa_B}\sin(\kappa_B\bar{b}) \\ \frac{\kappa_B}{\mu_B}\sin(\kappa_B\bar{b}) & \cos(\kappa_B\bar{b}) \end{bmatrix}$$
$$\times \begin{bmatrix} f_{j+1}(\xi_{2j}) \\ \frac{1}{\mu_A} f_{j+1}'(\xi_{2j}) \end{bmatrix}, \qquad (12)$$

where $j = 1, 2, \ldots, N - 1$. Moreover, by applying the boundary conditions for the electric field at the two last interfaces one may see that

$$\begin{bmatrix} f_N(\xi_{2N-1}) \\ \frac{1}{\mu_A} f_N'(\xi_{2N-1}) \end{bmatrix} = \begin{bmatrix} \cos(\kappa_B\bar{b}) & -\frac{\mu_B}{\kappa_B}\sin(\kappa_B\bar{b}) \\ \frac{\kappa_B}{\mu_B}\sin(\kappa_B\bar{b}) & \cos(\kappa_B\bar{b}) \end{bmatrix}$$
$$\times \begin{bmatrix} 1 & 1 \\ i\kappa_0 & -i\kappa_0 \end{bmatrix} \begin{bmatrix} E_t \\ 0 \end{bmatrix}. \qquad (13)$$

From Eqs. (9)–(13) it is possible to build a simple procedure to find the transmission coefficient. First we propose a value for E_t and obtain from Eq. (13) both $f_N(\xi_{2N-1})$ and $f_N'(\xi_{2N-1})$, which are used as boundary conditions to solve Eq. (5) in the interval (ξ_{2N-2},ξ_{2N-1}). Next we successively apply, from $j = N - 1$ to $j = 1$, Eq. (12) to find $f_j(\xi_{2j-1})$ as well as $f_j'(\xi_{2j-1})$, and then compute the electric field by solving Eq. (5) in the interval (ξ_{2j-2},ξ_{2j-1}). Finally, once the functions $f_1(\xi)$ and $f_1'(\xi)$ are obtained, we use Eq. (9) to find the value of E_i. The transmission coefficient may then be obtained through the expression

$$T = \left| \frac{E_t}{E_i} \right|^2. \qquad (14)$$

Notice that the reflection coefficient (results are not shown here) may be calculated as $R = \left| \frac{E_r}{E_i} \right|^2$, where E_r may also be

found from Eq. (9). Moreover, Eqs. (10) and Eqs. (11) may be used to obtain the coefficients C_j and D_j and, therefore, the electric field in the metamaterial regions through Eq. (8). For Fibonacci heterostructures of odd order the procedure to find the transmission and reflection coefficients is essentially the same. In such a case the Fibonacci sequence S_m always ends up with a letter A, and the last interface is located at ξ_{2N}, with $N = F_{m-2} + 1$.

III. RESULTS AND DISCUSSION

Let us begin by investigating the nonlinear properties of Fibonacci heterostructures in the frequency region around the zero-order gap. It should be noted here that the $\langle n \rangle$ average of the refractive index, for a Fibonacci sequence S_m, is defined as [11,12]

$$\langle n \rangle_m = \frac{\tau_m n_A a + n_B b}{\tau_m a + b}, \qquad (15)$$

with $\tau_m = \frac{N_A}{N_B}$, where N_A (N_B) is the number of A (B) layers in the S_m Fibonacci sequence and when $m \to \infty$, $\tau_m \to \tau$, with $\tau = \frac{1+\sqrt{5}}{2}$ being the Fibonacci-sequence golden mean. In this way, the $\langle n \rangle_m = 0$ gap for an S_m Fibonacci sequence occurs around the frequency satisfying the condition $\tau_m n_A a + n_B b = 0$ (see, for example, Fig. 4 by Bruno-Alfonso *et al.* [11]). One may notice that the $\langle n \rangle = 0$ frequency for the limiting condition in the case of large m is given when the optical paths in media A and B are in the golden ratio, i.e., $\frac{b|n_B|}{an_A} = \tau$. We have displayed in Fig. 2 the photonic band structure of periodic heterostructures with unit cells satisfying the Fibonacci building rule. Calculations were performed for normal incidence and obtained in the linear regime, with parameters $\epsilon_A = \epsilon_A^0 = 2$ and $\mu_A = 1$ in layers A. Absorption effects have not been considered in slabs B [$\gamma = 0$ in both Eqs. (2) and (3)]. It is apparent from Fig. 2 that the zero-order ($\langle n \rangle = 0$) gap stabilizes as the Fibonacci order m of the elementary cells increases, which agrees with predictions from Eq. (15) in the limit $\tau_m \to \tau$ as m increases.
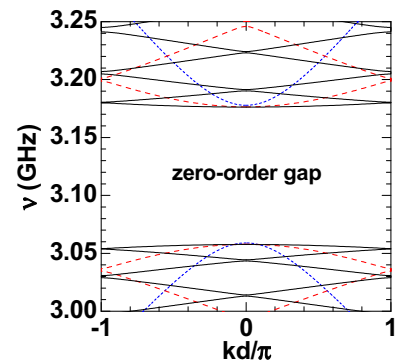
FIG. 2. (Color online) Photonic band structure, for normal incidence, of periodic heterostructures with unit cells satisfying the Fibonacci building rule with $a = b = 10$ mm. Results were obtained, in the vicinity of the zero-order ($\langle n \rangle = 0$) gap, by using $\epsilon_A = \epsilon_A^0 = 2$ [i.e., $\alpha = 0$ in Eq. (1)] and $\mu_A = 1$ in layers A, and $\gamma = 0$ in Eqs. (2) and (3) for slabs B. Solid, dashed, and dotted lines correspond to S_{12}, S_{10}, and S_8 Fibonacci heterostructures in the unit cell, respectively.
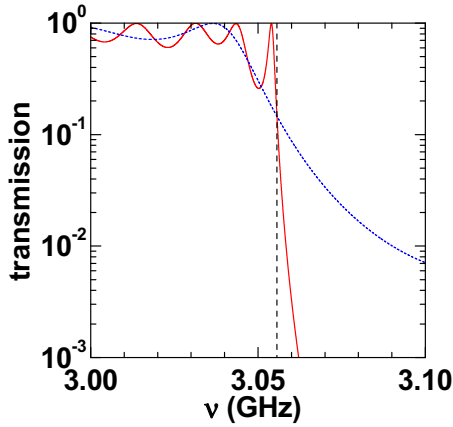
FIG. 3. (Color online) Transmission coefficient as a function of the wave frequency, for the same set of parameters used in Fig. 2. Dashed and solid lines correspond to the Fibonacci heterostructures S_{10} and S_{12}, respectively, with $a = b = 10$ mm. The vertical dashed line is located at $\nu = 3.0557$ GHz in the vicinity of the lower edges of the zero-order ($\langle n \rangle = 0$) gaps of the S_{10} and S_{12} Fibonacci heterostructures. At this frequency value the transmission coefficients of the S_{10} and S_{12} heterostructures coincide ($T = 0.1458$).

Having defined the frequency region where the zero-order gap is located for all m, we now calculate the transmission spectra for linear nondissipative systems in the case of an electromagnetic wave normally incident upon S_{10} and S_{12} Fibonacci heterostructures, whose building blocks A and B have equal widths, i.e., $a = b = 10$ mm. Results are displayed in Fig. 3; they were obtained by setting $\alpha = 0$ in Eq. (1) and $\gamma = 0$ in Eqs. (2) and (3). The vertical dashed line in Fig. 3 is at $\nu = 3.0557$ GHz in the vicinity of the lower edges of the $\langle n \rangle = 0$ gaps of the S_{10} and S_{12} Fibonacci heterostructures where the transmission coefficient $T = 0.1458$ is the same for both of them.

Let us now include both nonlinearity and absorption and loss effects and study the transmission coefficient depicted in Fig. 4 as a function of the nonlinearity, at the particular frequency $\nu = 3.0557$ GHz where the transmission coefficient is negligible in the linear regime. It is clear that the transmission-switching phenomenon occurs for both generations, i.e., S_{10} and S_{12}, although multistability is exhibited only in the case of the higher S_{12} generation sequence. In Fig. 5, the gap solitons corresponding to the first three points of maximum transmission for the S_{10} generation are plotted. For the lowest nonlinearity value a one-soliton distribution is clearly shown, although with low amplitude. The defocusing associated with the second point of maximum transmission gives rise to a two-soliton distribution, whereas defocusing corresponding to the third point of maximum transmission does not produce a clear three-soliton profile anymore. The effect of absorption in the case of $\gamma = 10^{-2}$ GHz washes out soliton formation. In contrast, for the S_{12} generation soliton formation is much clearer (see Fig. 6), and a comparison with the previous S_{10} generation results indicates that the S_{12} heterostructure system has been efficiently tuned so that the first three points of maximum transmission [cf. Fig. 3(b)] lead to one-, two-, and three-soliton solutions, respectively, even in the presence of
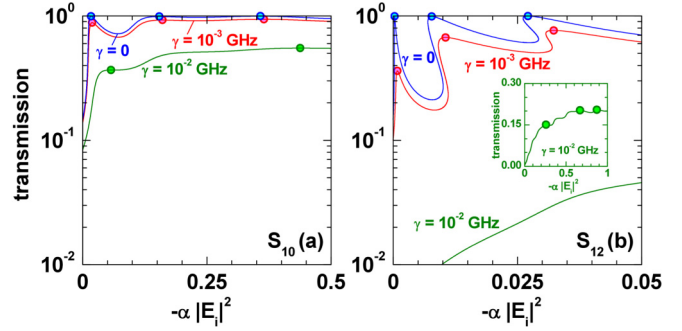
FIG. 4. (Color online) Transmission coefficient for normal incidence, as a function of the defocusing nonlinearity power, corresponding to the Fibonacci heterostructures (a) S_{10} and (b) S_{12}, with $a = b = 10$ mm. The linear parameters are the same as the ones used in Fig. 3. Results were obtained for $\nu = 3.0557$ GHz, in the vicinity of the bottom of the zero-order ($\langle n \rangle = 0$) gap (cf. the vertical dashed lines in Fig. 3). Calculations were performed for phenomenological loss and absorption parameters $\gamma = 0$, $\gamma = 10^{-3}$ GHz, and $\gamma = 10^{-2}$ GHz. In each panel, for each value of γ, dots are at the local maxima of the transmission coefficient. In the inset of (b) we have enlarged the interval of the defocusing nonlinearity power in order to display the three first local maxima of the transmission coefficient for $\gamma = 10^{-2}$ GHz.

absorption. Such solutions are quite robust to surface perturbations of a finite size and, in the present case, to perturbations induced by the quasiperiodicity of the structure. Therefore,
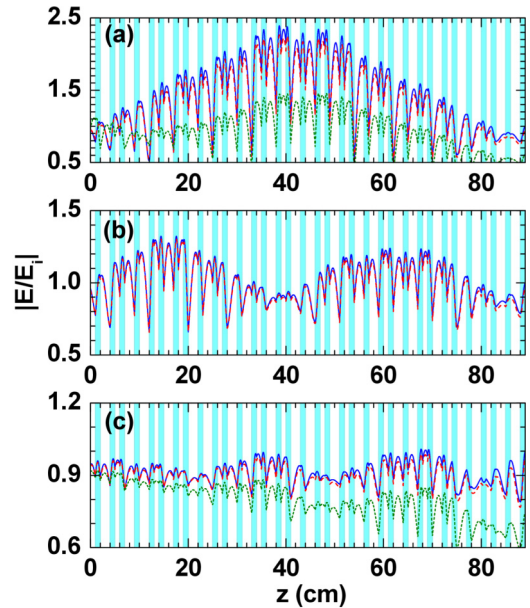
FIG. 5. (Color online) Zero-order ($\langle n \rangle = 0$) gap soliton for normal incidence corresponding to the first, second, and third local maxima [(a), (b), and (c), respectively] of the transmission as a function of the defocusing nonlinearity power [cf. Fig. 4(a)] in the S_{10} Fibonacci heterostructure with $a = b = 10$ mm at $\nu = 3.0557$ GHz. Solid, dashed, and dotted lines correspond to phenomenological loss and absorption parameters $\gamma = 0$, $\gamma = 10^{-3}$ GHz, and $\gamma = 10^{-2}$ GHz, respectively. Results for $\gamma = 10^{-2}$ GHz are not depicted in (b) because of the absence of the two-soliton peak in Fig. 4(a) for this level of absorption.
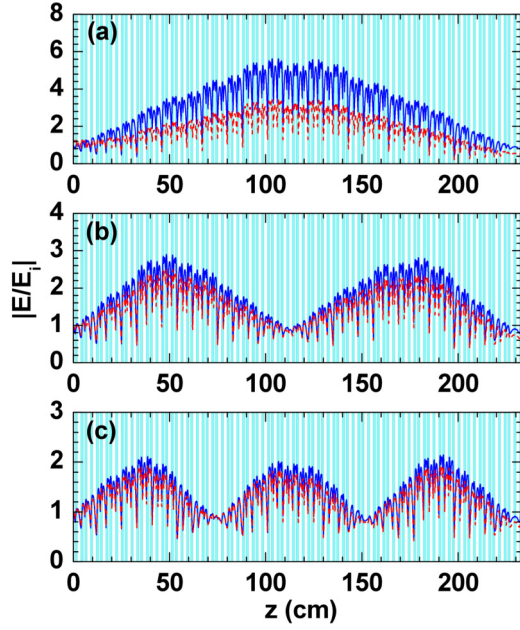
FIG. 6. (Color online) Zero-order ($\langle n \rangle = 0$) gap soliton for normal incidence corresponding to the first, second, and third local maxima [(a), (b), and (c), respectively] of the transmission as a function of the defocusing nonlinearity power [cf. Fig. 4(b)] in the S_{12} Fibonacci heterostructure with $a = b = 10$ mm at $\nu = 3.0557$ GHz. Solid and dashed lines correspond to phenomenological loss and absorption parameters $\gamma = 0$ and $\gamma = 10^{-3}$ GHz, respectively. Results for $\gamma = 10^{-2}$ GHz are not displayed because of the absence of the one-soliton, two-soliton, and three-soliton peaks in Fig. 4(b) for this level of absorption.

they should correspond to intrinsic resonance levels of the structure [8]. Actually, Chen and Mills [8] have demonstrated that, as the structure size decreases, one needs a higher threshold for the input power to excite the soliton, a fact that imposes a limiting size for observation of the soliton solution but that otherwise shows their existence in long enough finite systems.

Here, it is important to discuss the localization properties of solitons in the Fibonacci heterostructure. In that respect, let us introduce the inversion operator $\hat{I}_{z_0}$ such that $\hat{I}_{z_0} f(z - z_0) = f(z_0 - z)$, where f is an arbitrary continuous function. One may easily see that the eigenvalues of the inversion operator are $\iota = \pm 1$ and, therefore, its corresponding eigenfunctions are even or odd functions of $z - z_0$. Now let us suppose that the slab distribution in the Kerr-metamaterial heterostructure has an inversion center at $z = z_0$. As a consequence, $\mu = \mu(z)$ in Eq. (4) is an even function of z with respect to z_0. In addition, the stepwise electric permittivity may be rewritten as

$$\epsilon(z) = \epsilon_0(z) + \alpha \Theta(z)|E(z)|^2, \tag{16}$$

where

$$\epsilon_0(z) = \begin{cases} \epsilon_A^0 & \text{if} \quad z \in A, \\ \epsilon_B & \text{if} \quad z \in B, \end{cases} \tag{17}$$

and

$$\Theta(z) = \begin{cases} 1 & \text{if} \quad z \in A, \\ 0 & \text{if} \quad z \in B, \end{cases} \tag{18}$$

are also even functions of $z - z_0$. Bearing the above results in mind one may straightforwardly show that, provided there exists an inversion center at the point z_0 in the heterostructure, then both the electric-field amplitude E and $\hat{I}_{z_0} E$ satisfy the same Eq. (4). Therefore, the absolute value of the electric-field amplitude will be an even function of $z - z_0$ if the condition $|E_i| = |\iota E_t|$ is fulfilled or, in other words, if $T = 1$. Strictly speaking, a Fibonacci heterostructure has not an inversion center. However, as explained, for $m \geqslant 4$ the heterostructure Ω_m resulting from suppressing the two last elements of S_m has an inversion center at the middle of the heterostructure (see Fig. 1). As the Fibonacci order m increases, the heterostructure Ω_m becomes a good representation of S_m and, therefore, the solutions of Eq. (4) increasingly look like symmetrical functions of z with respect to the inversion center of Ω_m. This behavior may be clearly observed in both Figs. 5 and 6, and is similar to those observed in periodic heterostructures [9,10]. In this sense, the localization properties of zero-order gap solitons are not essentially affected by quasiperiodicity as compared with the periodic case, a fact with may be understood from the weak dependence of the zero-order gap profile on the Fibonacci order (see Fig. 2).

Let us proceed to investigate nonlinear switching and soliton formation inside the TE longitudinal magnetic PP gap [5] for the case of Fibonacci heterostructures [13]. To this end we display in Fig. 7 the photonic band structure of periodic heterostructures with unit cells satisfying the Fibonacci building rule. Results were obtained for frequency values around the PP gap for oblique incidence with $\theta = \pi/24$ in the TE configuration, in the linear regime, and in the absence of absorption. We set $\epsilon_A = \epsilon_A^0 = 2$ and $\mu_A = 1$ in layers A, and $a = b = 10$ mm. Solid, dashed, and dotted lines correspond to S_6, S_4, and S_2 Fibonacci heterostructures in the unit cell, respectively. The physical origin of the PP gap stems from the fact that, in a TE configuration and for oblique incidence, there is a magnetic-field component in the stacking direction which couples the photon mode to the bulklike longitudinal
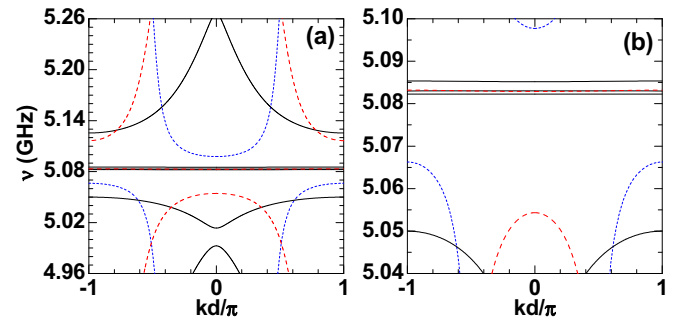
FIG. 7. (Color online) Photonic band structure for oblique incidence ($\theta = \pi/24$) and TE configuration in the linear regime [$\alpha = 0$ in Eq. (1)] of periodic heterostructures with unit cells satisfying the Fibonacci building rule. Results were obtained for frequency values around the PP gap, with parameters $\epsilon_A = \epsilon_A^0 = 2$ and $\mu_A = 1$ in layers A, $\gamma = 0$ in Eqs. (2) and (3) for slabs B, and $a = b = 10$ mm. Solid, dashed, and dotted lines correspond to S_6, S_4, and S_2 Fibonacci heterostructures in the unit cell, respectively. (b) displays a zoom of the numerical results depicted in (a) around the PP gap, in order to capture the fine details of the band structure.
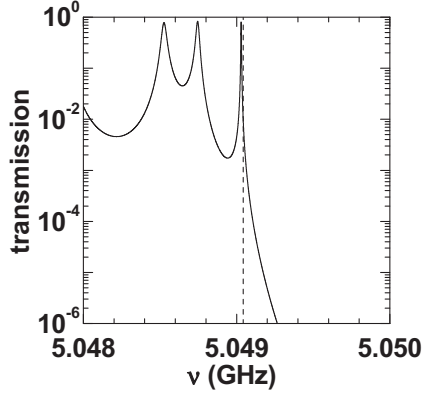
FIG. 8. Transmission coefficient for the TE configuration with incidence angle $\theta = \pi/24$, as a function of the wave frequency, for $\alpha = 0$ in Eq. (1) and $\gamma = 0$ in Eqs. (2) and (3). The calculated result corresponds to the Fibonacci heterostructure S_{12}, with $a = b = 10$ mm. The vertical dashed line is located at $\nu = 5.0490$ GHz in the vicinity of the lower edge of the TE longitudinal magnetic PP gap. At this frequency value one has $T = 0.01$.

ν_m^p magnetic plasmon mode ($\mu_B = 0$ at $\nu_m^p = 5.0807$ GHz). As is well known [13], in 1D photonic superlattices in which Fibonacci sequences S_m play the role of elementary cells, the number of PP subbands—corresponding to the coupling of photons and plasmons—appearing for oblique incidence is just the number of metamaterial layers contained in S_m. This has an effect in the optical properties related to the PP gap including, of course, the transmission-switching phenomenon as well as the localization properties of PP gap solitons.

We display in Fig. 8 the linear TE transmission in the absence of losses, for $\theta = \pi/24$, in the vicinity of the lower-frequency edge of the magnetic PP gap. Notice the vertical dashed line in Fig. 8, which essentially indicates the $\nu = 5.0490$ GHz frequency in the vicinity of the lower edge of the PP gap for which the transmission becomes negligibly small ($T = 0.01$). By including effects of nonlinearity and loss, one is able to study the transmission switching and multistability phenomena [10]. The transmission switch to a maximum value for various discrete values of the incident power, for different values of the phenomenological loss and

absorption γ parameters of the metamaterial (layers B), is illustrated in Fig. 9, for the S_{12} Fibonacci heterostructure, with $a = b = 10$ mm. It is apparent in Fig. 9 that the defocusing nonlinearity leads to several transmission maxima at specific field-intensity values for $\nu = 5.0490$ GHz in the vicinity of the lower edge of the TE magnetic PP gap. As we have depicted in Fig. 7, as the Fibonacci order of the heterostructure is increased, there occurs a splitting of the PP modes in the vicinity of the plasmon frequency. Such splitting is caused by the absence of long-range spatial coherence of the PP modes due to the quasiperiodicity [13]. The quasiperiodicity of the heterostructure may therefore considerably affect the way in which the transmission-switching phenomenon takes place in this particular case and, in fact, originates the presence of multiple maximum-transmission peaks with different heights, as shown in Fig. 9.

Here, one may point out that linear theory asserts the existence of PPs, and the very physical mechanism that explains the PP gap, the region where photons couple with plasmons. Therefore, the transmission switching at particular power values may be interpreted as a consequence of the resonant excitation of a soliton that lies inert in the lattice ready for an incoming wave with the right power to excite it. Alternatively, one may think of it as a nonlinear mode being excited by the incident electric field so that the amplitude of the reflected wave is zero and all the energy flows through the finite superlattice.

In contrast with zero-order gap solitons, the understanding of the localization properties of the PP gap solitons is somewhat tricky. Figure 10 displays the calculated solutions for TE longitudinal magnetic PP gap solitons for oblique incidence ($\theta = \pi/24$) in the Fibonacci heterostructure S_{12}, with $a = b = 10$ mm. Calculations were performed for the first five local maxima of the transmission coefficient, as labeled in Fig. 8, and taking into account loss and absorption effects via the phenomenological damping parameters $\gamma = 0$, $\gamma = 10^{-5}$ GHz, and $\gamma = 10^{-4}$ GHz. The results depicted in Figs. 10(a), 10(c), and 10(e) may be interpreted in terms of solutions corresponding to one-soliton, two-soliton, and three-soliton solutions, respectively, and their corresponding absolute values of the electric-field amplitudes essentially behave as even functions of the coordinate z with respect to the inversion center of the S_{12} heterostructure. However, the
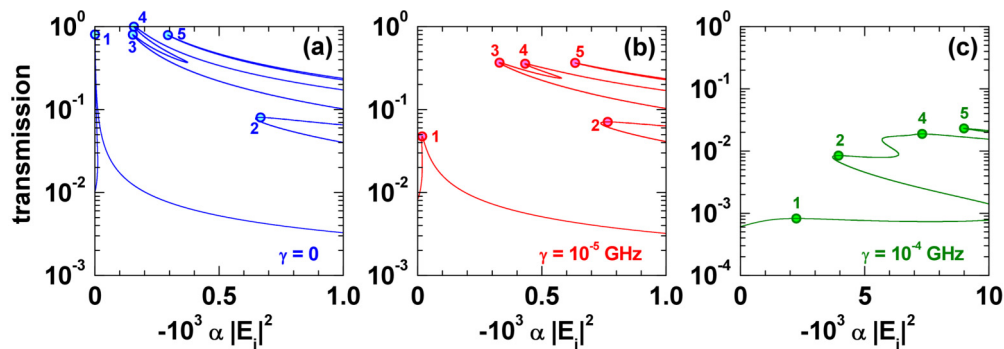
FIG. 9. (Color online) Transmission coefficient of the TE modes with incidence angle $\theta = \pi/24$ as a function of the defocusing nonlinearity power in the Fibonacci heterostructure S_{12}, with $a = b = 10$ mm. Results were obtained at $\nu = 5.0490$ GHz in the vicinity of the lower edge of the TE PP gap (cf. the vertical dashed line in Fig. 8), and for three different values of the phenomenological loss and absorption parameters γ of layers B. In all panels, for each value of γ, dots are located at the local maxima of the transmission coefficient.
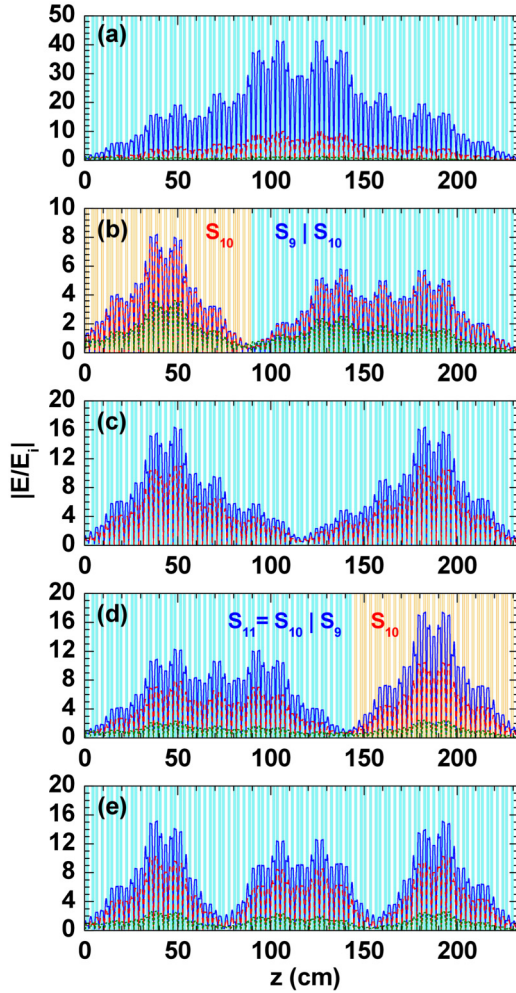
FIG. 10. (Color online) TE plasmon-polariton gap solitons for oblique incidence ($\theta = \pi/24$) in the Fibonacci heterostructure S_{12}, with $a = b = 10$ mm. Solid, dashed, and dotted lines correspond to phenomenological loss and absorption parameters $\gamma = 0$, $\gamma = 10^{-5}$ GHz, and $\gamma = 10^{-4}$ GHz, respectively. Results corresponding to the different values of the damping constant γ were obtained for the first five local maxima of the transmission coefficient as labeled in Fig. 9.

results shown in both Figs. 10(b) and 10(d) do not follow this simple interpretation. The effects of the quasiperiodicity of the heterostructure are quite appreciable in these cases. According to the inflation law used to generate the Fibonacci sequences, it is clear that $S_{12} = S_{11}|S_{10} = S_{10}|S_9|S_{10}$. One may note that the heterostructure resulting from removing the two last elements AB from $S_9|S_{10}$ has an inversion center at the middle of the system. The two-soliton solution depicted in Fig. 10(b) may be interpreted as the superposition of two single solitons, one localized at the inversion center of the first S_{10} heterostructure and the other one localized at the inversion center of the concatenated heterostructure $S_9|S_{10}$. The absolute values of the electric-field amplitudes of each of the single solitons are even functions with respect to the corresponding inversion centers. A similar situation may be observed in Fig. 10(d), where the localization takes places around the inversion centers of the heterostructures S_{11} and S_{10} composing the entire system

S_{12}. In other words, the localization properties of PP gap solitons in a Fibonacci heterostructure are essentially related to the quasiperiodicity dependence of the PP gap properties.

In the present study we have considered a defocusing nonlinearity as we have chosen a frequency region in the vicinity of the lower edge of the non-Bragg gaps. This type of switching behavior is found in this frequency region in the case of a self-defocusing nonlinearity. To observe the same switching phenomena with a focusing nonlinearity one should choose a frequency in the vicinity of the upper edge [8]. In both cases the same behavior is essentially found so that the results obtained in the present work may be inferred in the self-focusing case, except that the frequency chosen should be at the upper gap edge. Actually, one may conjecture that this selection of the gap edge according to the type of nonlinearity is due to the dynamical shift in the location of the band gap [17], which is known to be dependent on the difference of the refractive index of the alternating layers.

Finally, we stress that all results here discussed for TE electromagnetic modes have, of course, a similar counterpart for TM modes in the vicinity of the electric PP gap.

IV. CONCLUSIONS

Summing up, we have carried out an investigation of the nonlinear properties of non-Bragg gaps in 1D Kerr-metamaterial quasiperiodic Fibonacci heterostructures. Calculations were performed by combining the transfer-matrix formalism in the metamaterial layers together with a numerical solution of the nonlinear differential equation corresponding to the TE modes in the Kerr slabs.

By considering both nonlinearity and absorption effects in the metamaterial slabs, we have studied the transmission properties of both S_{10} and S_{12} Fibonacci heterostructures as a function of the defocusing nonlinearity power in the vicinity of the zero-order gap, for frequency values corresponding to a negligible transmissivity in the linear regime and for normal incidence. In all cases we demonstrated that the system transmissivity switches from a state of no transparency, in the linear regime, to high-transparency states in the nonlinear regime, whereas multistability is exhibited only in the case of the S_{12} generation sequence. The results reported here suggest that the effects of the quasiperiodicity do not considerably affect the spatial-localization properties of the zero-order gap solitons in the heterostructure.

We have also performed a similar study for frequency values in the vicinity of the magnetic PP gap for oblique incidence with $\theta = \pi/24$ in the TE configuration. The splitting of the PP modes in the vicinity of the plasmon frequency affects the way in which transmission switching occurs, and multiple maximum-transmission peaks with different heights appear when the transmission coefficient is plotted as a function of the defocusing nonlinearity power. The magnetic PP gap solitons exhibit, in some cases, a strong localization around the inversion center of the entire system, whereas in other cases they localize around the inversion centers corresponding to Fibonacci sequences of lower order which are contained in the heterostructure. The localization properties of the PP gap solitons are a clear manifestation of the quasiperiodicity

in the electromagnetic modes in Kerr-metamaterial Fibonacci heterostructures.

Finally, we would like to point out that, in all cases studied in the present work, the transparency-switching phenomenon is still observable at low levels of loss and absorption in the heterostructure. Of course, high levels of loss and absorption [$\gamma^2 \gg \beta_\epsilon$ and $\gamma^2 \gg \beta_\mu$ in Eqs. (2) and (3), respectively] may cause full extinction of the soliton waves in the heterostructure and a flattening of the soliton-induced transmission peaks

in the nonlinearity-power dependence of the transmission coefficient.

[1] V. G. Veselago, Sov. Phys. Usp. **10**, 509 (1968); R. A. Shelby, D. R. Smith, and S. Schultz, Science **292**, 77 (2001); W. L. Barnes, A. Dereux, and T. W. Ebbesen, Nature (London) **424**, 824 (2003).

[2] S. A. Ramakrishna, Rep. Prog. Phys. **68**, 449 (2005); E. Ozbay, Science **311**, 189 (2006); J. B. Pendry, D. Schurig, and D. R. Smith, *ibid.* **312**, 1780 (2006).

[3] J. Li, L. Zhou, C. T. Chan, and P. Sheng, Phys. Rev. Lett. **90**, 083901 (2003); H. Jiang, H. Chen, H. Li, Y. Zhang, and S. Zhu, Appl. Phys. Lett. **83**, 5386 (2003).

[4] J. Elser and V. A. Podolskiy, Phys. Rev. Lett. **100**, 066402 (2008).

[5] E. Reyes-Gómez, D. Mogilevtsev, S. B. Cavalcanti, C. A. A. Carvalho, and L. E. Oliveira, Europhys. Lett. **88**, 24002 (2009); C. A. A. de Carvalho, S. B. Cavalcanti, E. Reyes-Gómez, and L. E. Oliveira, Phys. Rev. B **83**, 081408(R) (2011).

[6] Y. V. Kartashov, B. A. Malomed, and L. Torner, Rev. Mod. Phys. **83**, 247 (2011).

[7] M. Lapine, I. V. Shadrivov, and Y. S. Kivshar, Rev. Mod. Phys. **86**, 1093 (2014).

[8] W. Chen and D. L. Mills, Phys. Rev. Lett. **58**, 160 (1987); Phys. Rev. B **36**, 6269 (1987).

[9] R. S. Hedge and H. G. Winful, Microwave Opt. Technol. Lett. **46**, 528 (2005); Opt. Lett. **30**, 1852 (2005).

[10] S. B. Cavalcanti, P. A. Brandão, A. Bruno-Alfonso, and L. E. Oliveira, Opt. Lett. **39**, 178 (2014); E. Reyes-Gómez, S. B. Cavalcanti, and L. E. Oliveira, Europhys. Lett. **106**, 64001 (2014).

[11] A. Bruno-Alfonso, E. Reyes-Gómez, S. B. Cavalcanti, and L. E. Oliveira, Phys. Rev. A **78**, 035801 (2008).

[12] J. A. Monsoriu, R. A. Depine, M. L. Martìnez-Ricci, E. Silvestre, and P. Andrés, Opt. Lett. **34**, 3172 (2009).

[13] E. Reyes-Gómez, N. Raigoza, S. B. Cavalcanti, C. A. A. de Carvalho, and L. E. Oliveira, Phys. Rev. B **81**, 153101 (2010); J. Phys.: Condens. Matter **22**, 385901 (2010).

[14] S. B. Cavalcanti, M. de Dios-Leyva, E. Reyes-Gómez, and L. E. Oliveira, Phys. Rev E. **75**, 026607 (2007).

[15] T. Peschel, P. Dannberg, U. Langbein, and F. Lederer, J. Opt. Soc. Am. B **5**, 29 (1988); U. Trutschel and F. Lederer, *ibid.* **5**, 2530 (1988).

[16] S. D. Gupta, J. Opt. Soc. Am. B **6**, 1927 (1989).

[17] M. Scalora, J. P. Dowling, C. M. Bowden, and M. J. Bloemer, Phys. Rev. Lett. **73**, 1368 (1994).